Enhancing Archaeological Insights: Role of Mössbauer Spectroscopy in Characterizing the Wall and Red Pigment of Tomb No. 63 of the Gaya Tumuli

Hyunkyung Choi¹, Min Su Han², Gwang-Min Sun¹, and Young Rang Uhm^{1*}

¹HANARO Utilization Division, Korea Atomic Energy Research Institute (KAERI), Daejeon 34057, Republic of Korea ²Department of Heritage Science and Technology Studies, Graduate School of Cultural Heritage, Korea National University of Heritage, Buyeo 33115, Republic of Korea

(Received 4 August 2025, Received in final form 28 August 2025, Accepted 29 August 2025)

This study explores the contributions of Mössbauer spectroscopy in characterizing the wall and red pigments used in Tomb No. 63 of the Gaya tumuli. Mössbauer spectroscopy, chromaticity, X-ray diffraction, and magnetic property analyses were employed to analyze iron oxides and (oxy)hydroxides in the red pigment and walls. Room-temperature Mössbauer spectroscopy analyses confirmed hematite as the primary component of the red pigment. The red pigment exhibited weak ferromagnetic behavior, whereas the walls displayed antiferromagnetic properties. Furthermore, the quadrupole splitting value from low-temperature Mössbauer spectroscopy indicated the absence of ferrihydrite and presence of superparamagnetic goethite in the walls. These findings provide crucial insights into environmental changes within the tomb and demonstrate the effectiveness of Mössbauer spectroscopy in distinguishing iron mineral phases in complex soil matrices. Moreover, this technique proves useful in archaeology by enhancing our understanding of red pigments and past soil environments.

Keywords: Mössbauer spectroscopy, red pigment, Gaya tumuli, hematite, goethite, ferrihydrite

1. Introduction

The Bihwa Gaya tumuli, located in Gyo-dong and Songhyeon-dong, Changnyeong-gun, Gyeongsangnam-do (South Korea), dates back to the Gaya period, constructed between the mid-5th and early 6th centuries [1]. Inside Tomb No. 63, researchers found red pigment painted on the walls, likely used symbolically to ward off evil spirits. To better understand the tomb's historical and environmental context, it is necessary to investigate the pigment and wall on which it was painted. Tomb interiors undergo prolonged changes influenced by environmental factors such as humidity and temperature [2]. Studying the iron oxides and (oxy)hydroxides within the walls and pigment can provide insights into these environmental conditions. Ferric hydroxide, a common iron-bearing mineral found in soil, is an indicator of past environmental conditions, particularly those related to soil formation and moisture exposure [3]. Tombs, typically constructed from soil or stone to protect from external elements, lack ventilation and drainage, leading to prolonged humidity that gradually transforms poorly crystalline ferrihydrite (Fe₂O₃·nH₂O) into crystalline goethite (α -FeOOH) [4]. The main reaction is as follows:

$$Fe_2O_3 \cdot nH_2O \rightarrow 2\alpha - FeOOH + (n-1)H_2O$$
 (1)

Sufficient water (H₂O) promotes structural rearrangement of ferrihydrite, as water stabilizes Fe-OH bonds and fosters new goethite nuclei [5]. In humid soils, amorphous ferrihydrite tends to dissolve and reprecipitate as goethite [6, 7]. Interactions with organic matter or silica (SiO₂) can inhibit this transformation, allowing ferrihydrite to persist longer [8]. Ferrihydrite often converts to lepidocrocite in environments with frequent redox cycles [9]. In contrast, arid environments, such as sandy soil, with limited water allow ferrihydrite to remain stable for extended periods, as the dryness prevents significant rearrangement of iron oxides, allowing ferrihydrite to persist in its low-crystalline form [10]. In dry, high-temperature conditions, ferrihydrite can slowly transform into hematite but at an extremely slow rate [11]. Therefore, ferrihydrite converts

©The Korean Magnetics Society. All rights reserved. *Corresponding author: Tel: +82-42-868-4835 Fax: +82-42-868-8448, e-mail: uyrang@kaeri.re.kr to goethite at low to moderate temperatures and remains stable in acidic (pH 2–5) or alkaline (pH 10–14) environments, whereas conversion to hematite is more active at high temperatures and neutral pH 7 [5, 6]. The transformation pathways of ferrihydrite vary significantly with environmental conditions, and analyzing these changes provides valuable insights into past climate and soil conditions [11]. Thus, ferrihydrite and goethite yield crucial information for interpreting environmental changes within the tomb.

Distinguishing (oxy)hydroxides in complex soil environments pose challenges because of their low crystallinities [12]. Although X-ray diffraction (XRD) can detect crystalline phases, it often fails to differentiate between amorphous and nanocrystalline iron oxides [13]. Additionally, scanning and transmission electron microscopy may face limitations related to low concentrations and small particle sizes. Mössbauer spectroscopy, which utilizes nuclear resonant absorption and emission of gamma rays by iron nuclei, is an effective alternative for distinguishing iron oxidation states and mineral phases, even in complex matrices that confound conventional methods [14-16].

This study employs Mössbauer spectroscopy with complementary analytical techniques to characterize the magnetic and structural properties of iron oxides and (oxy)hydroxides found in the red pigment and walls of an ancient tomb. The primary aim was to trace environmental influences on the tomb over time and offer insights into the long-term preservation of archaeological contexts. This approach not only enhances our understating of the formation and transformation process of iron oxides but also improves the accuracy of mineral identification in natural samples, contributing to archaeological insights.

2. Experimental

2.1. Materials: Red pigment and wall from Tomb No. 63

Figure 1 depicts the wall and red pigment painted to its surface, uncovered in Tomb No. 63 of the Gaya tumuli. The red pigment was applied thinly to the inner walls of the tomb. For the three samples collected, the wall and red pigment were categorized as follows: W-1, W-2, and W-3 for the wall, and R-1, R-2, and R-3 for the red pigment. All samples were collected as powders.

2.2. Reagents

All reagents were purchased commercially and used without further purification. Hematite, wüstite, magnetite, and goethite were purchased from Sigma-Aldrich, whereas lepidocrocite was sourced from Thermo Fisher Scientific.



Fig. 1. (Color online) Location of the archaeological Gaya tumuli and an image of a red pigment on the wall of Tomb No. 63

Ferrihydrite was synthesized using a previously reported method [17].

2.3. Methods

Chromaticity was measured using a UV-VIS spectrophotometer (UV-2450 Shimadzu) equipped with an MPC-2200. Commission International d'Eclairge (CIE) L*, a*, and b* values were recorded to quantify the brightness and saturation of the red pigment. Chromaticity measurements were conducted on the uncontaminated sections of the red pigment, averaging over 10 measurements. XRD analyses were conducted using a Bruker D2 phaser XE-T with Cu-Kα radiation to determine the mineralogical composition. XRD patterns were collected over a 20 range of 5°-80°. Magnetic properties were assessed through M-H curves recorded using a vibrating sample magnetometer (VSM, Lake Shore7404 model) in fields up to 20 kOe. The Mössbauer spectra were recorded at room temperature (RT) using a transmission spectrometer in constant acceleration mode with a ⁵⁷Co/Rh source, calibrated with α -Fe as a standard and fitted with Lorentzian lines. Low-temperature Mössbauer measurements were performed at 4.2 K using a helium closed-cycle cryo-refrigerator.

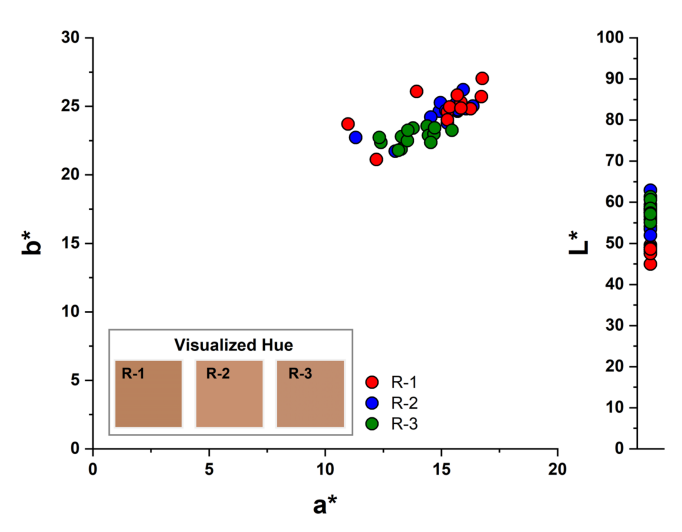


Fig. 2. (Color online) Chromaticity diagrams of red pigments R-1, R-2, and R-3.

3. Results and Discussion

Chromaticity was used to quantify the color of the red pigment in Tomb No. 63, with the corresponding diagram shown in Fig. 2. Ancient pigments consist of non-uniform particles and uneven distributions, requiring multiple chromaticity measurements to obtain accurate color values. Colorimetry followed the L*a*b* model proposed by CIE. The average L* values of the red pigment were 50.55, 57.60, and 58.05 for samples R-1, R-2, and R-3, respectively. The average a* and b* values, which ranges from green (-a*) to red (+a*), and blue (-b*) to yellow (+b*), respectively, are as follows. For R-1, R-2, and R-3, the a* values were 15.07, 14.99, and 13.83, while the b* values were 24.86, 24.45, and 22.80, respectively. The recorded CIE L*a*b* values were visualized as hues, as shown in Fig. 2.

Figures 3a and b display the XRD patterns of the walls (W-1, W-2, and W-3) inside the tomb and red pigments (R-1, R-2, and R-3) on its surface. The wall samples are mainly composed of quartz, plagioclase, alkali feldspar, and chlorite, whereas the red pigment samples consist of quartz and amorphous phase. In the XRD patterns, the broad peaks observed around 20° and 35° 2θ correspond to the typical diffraction features of mica group minerals. However, the characteristic 10 Å peak of mica was not clearly observed in Fig. 3. This absence is likely due to limitations in sample preparation, such as insufficient grinding or an inadequate amount of powdered sample, rather than the complete absence of mica. Additionally, a broad, low-intensity peak in Fig. 3b suggests the presence of an amorphous or poorly crystalline substance, such as

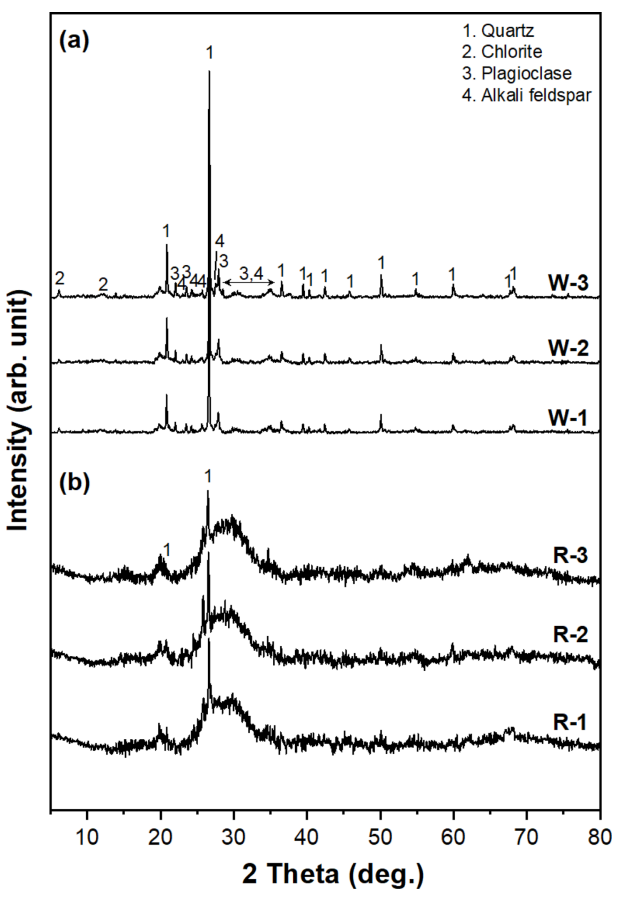


Fig. 3. XRD patterns of the (a) walls (W-1, W-2, and W-3) and (b) red pigments (R-1, R-2, and R-3).

ferrihydrite or superparamagnetic nanogoethite [18, 19].

In general, hematite is most likely the primary mineral responsible for the red pigment. However, no other iron oxides or hydroxides were detected in the XRD of the wall or red pigment, likely because iron oxides in soil typically exist as low-crystallinity nanoparticles [12]. Therefore, the magnetic properties of the samples were investigated to better identify the iron oxide crystals present. Figs. 4a and b show the hysteresis curves of the red pigments and walls, which reveal distinct magnetic properties. The red pigment exhibits weak ferromagnetic behavior, characteristic of certain iron oxides such as hematite, while the wall exhibits linear behavior across the measured magnetic field range, indicative of antiferromagnetic properties of some iron oxyhydroxides. The enlarged W-3 sample (inset in Fig. 4b) reveals a slightly nonlinear behavior near H=0, suggesting the presence of canted spins in antiferromagnetic goethite [20, 21].

To identify the iron oxides and (oxy)hydroxides present in the samples accurately, the hysteresis curves for the following reference samples were measured (Fig. 5): iron

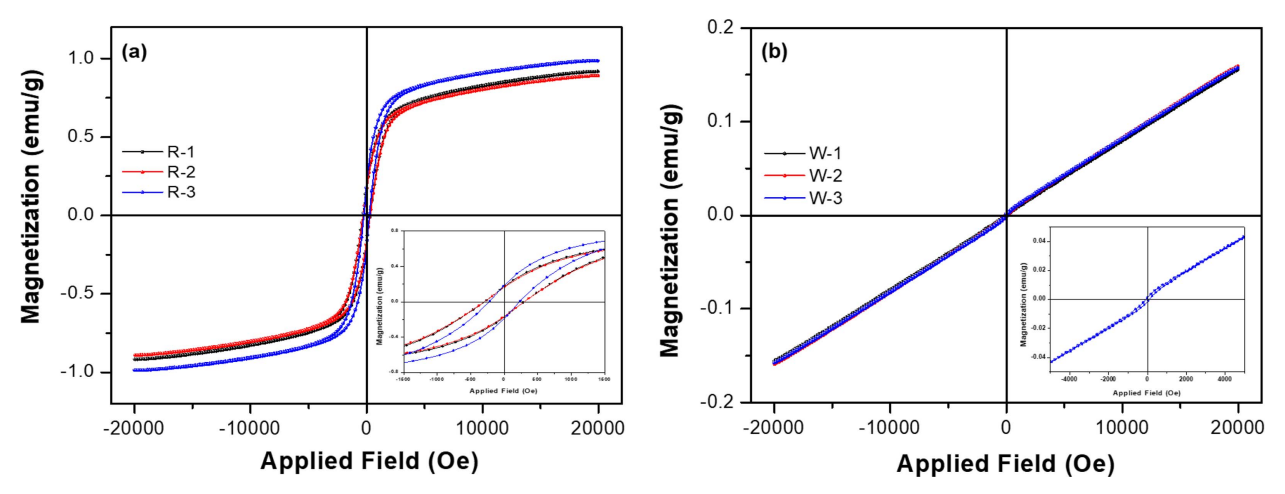


Fig. 4. (Color online) Hysteresis curves with enlarged images: (a) red pigments and (b) walls.

oxides (hematite, wüstite, and magnetite), iron oxyhydroxides (goethite and lepidocrocite), and iron hydroxides (ferrihydrite). In Fig. 5a, hematite exhibits weak ferromagnetic behavior owing to its canted spin structure, resulting in a small net magnetic moment [22]. Moreover, it does not reach saturation magnetization even at a magnetic field of 20 kOe. Ideal wüstite exhibits a linear increase in magnetization under an external magnetic field and typically exhibits no hysteresis. However, oxygen

vacancies or Fe³⁺ ions in the lattice structure can induce weak ferromagnetic-like behavior [23]. Fig. 5b reveals wüstite's slight hysteresis curve and residual magnetization, likely due to these impurities or structural defects. Magnetite, which is ferrimagnetic, exhibits a hysteresis curve with high saturation magnetization (Fig. 5c). Goethite is antiferromagnetic at RT, exhibiting linear behavior with no observed hysteresis, although it may exhibit weak hysteresis curve due to canted spins or defects. In Fig. 5d, goethite

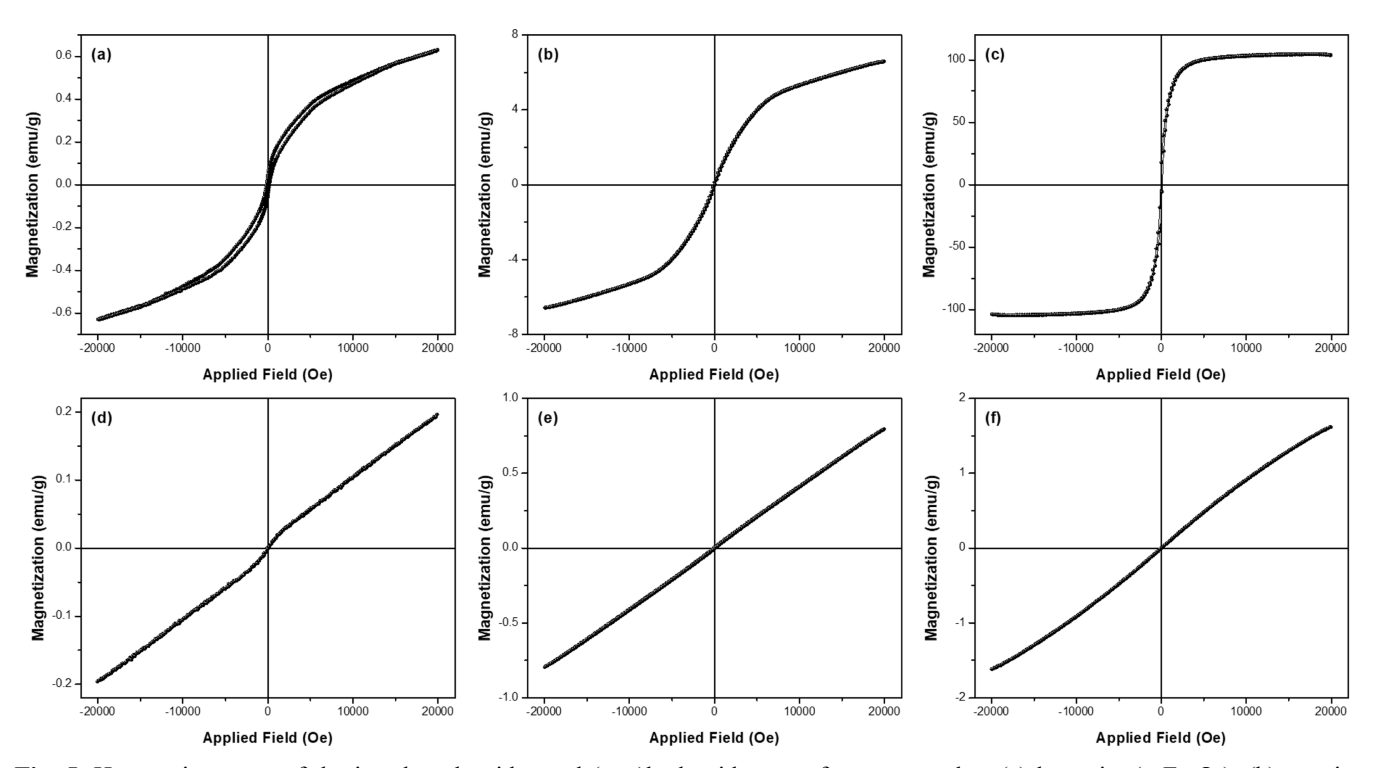


Fig. 5. Hysteresis curves of the iron-based oxides and (oxy)hydroxides as reference samples: (a) hematite (α -Fe₂O₃), (b) wüstite (Fe_xO), (c) magnetite (Fe₃O₄), (d) goethite (α -FeOOH), (e) lepidocrocite (γ -FeOOH), and (f) ferrihydrite (Fe₂O₃·nH₂O).

Table 1. Hysteresis parameters of the red pigments (R-1, R-2, and R-3), walls (W-1, W-2, and W-3), and reference samples.

Sample	M (emu/g)	M _r (emu/g)	H _c (Oe)		
R-1	0.917	0.170	292.67		
R-2	0.890	0.165	297.44		
R-3	0.986	0.186	225.85		
W-1	0.155	0.002	84.422		
W-2	0.159	0.002	98.389		
W-3	0.157	0.002	94.475		
Hematite	0.630	0.041	138.08		
Wüstite	6.588	0.119	78.428		
Magnetite	103.9	17.83	99.700		
Goethite	0.196	0.002	87.842		
Lepidocrocite	0.794	0.001	25.567		
Ferrihydrite	1.616	0.003	19.966		

exhibits linear behavior within the measured magnetic field range but shows nonlinear behavior at low magnetic fields, likely due to the presence of superparamagnetic goethite [24]. Lepidocrocite remains paramagnetic at RT and maintains a linear relationship with the applied magnetic field (Fig. 5e). Ferrihydrite approaches linear

behavior at RT; however, a detailed examination reveals slight hysteresis (Fig. 5f). The parameters derived from the hysteresis curves in Figs. 4 and 5, including magnetization (M) at 20 kOe, remanent magnetization (M_r), and coercivity (H_c), are summarized in Table 1. The hysteresis curves show that the red pigment exhibits a magnetic behavior similar to that of hematite, whereas the wall shows a behavior similar to that of goethite. However, goethite and ferrihydrite exhibit similar linear behaviors under an applied magnetic field. At 20 kOe, the M value of ferrihydrite (1.616 emu/g) significantly exceeds that of goethite (0.196 emu/g) and the wall (0.15 emu/g). The reduced magnetization of the wall compared to that of pure goethite results from the partial substitution of Fe³⁺ sites in the goethite lattice by impurities such as Al³⁺, Si⁴⁺, and Mn²⁺ ions during soil formation, with nonmagnetic Al3+ ions being predominant [25]. Based on the VSM results, we have inferred the presence of superparamagnetic goethite while excluding ferrihydrite within the wall. These findings underscore the significance of the unique magnetic properties of iron-based oxides and (oxy)hydroxides as indicators in archaeological research.

Figure 6 presents the RT Mössbauer spectra of the (a) walls (W-1, W-2, and W-3) and (b) red pigments (R-1, R-

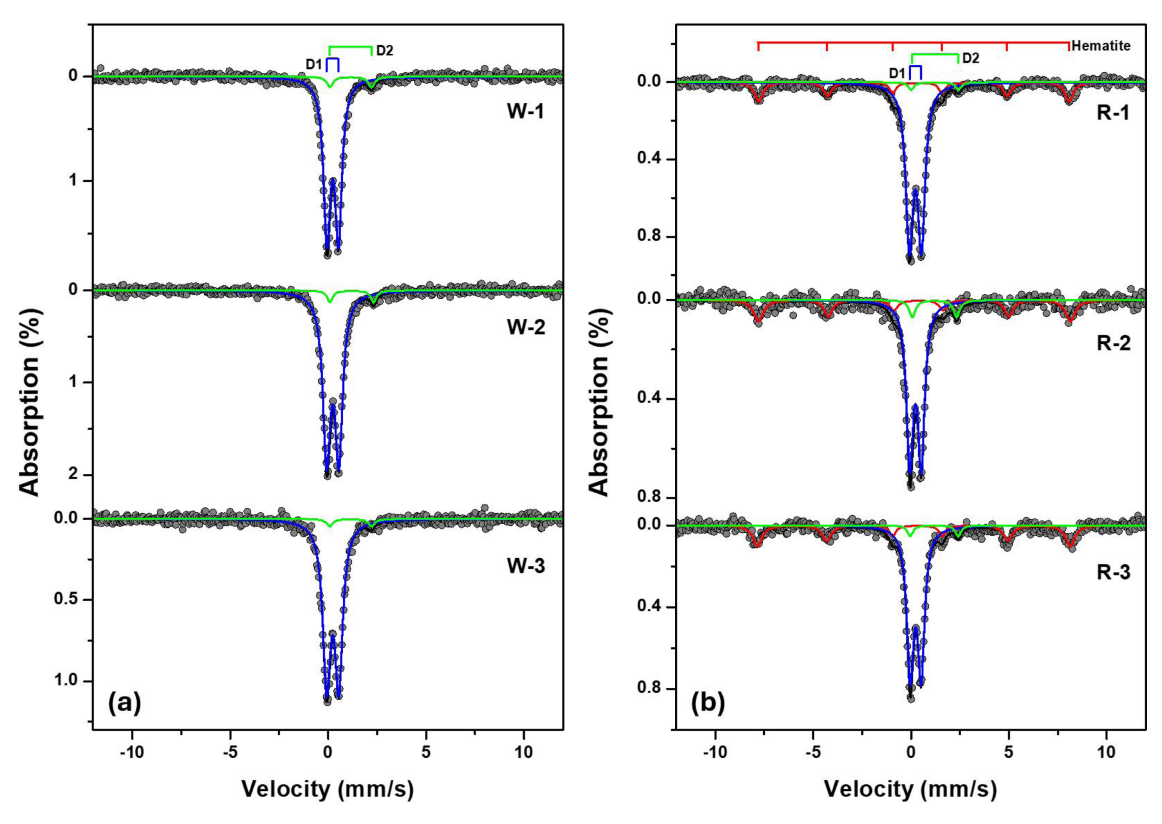


Fig. 6. (Color online) Mössbauer spectra of (a) walls (W-1, W-2, and W-3) and (b) red pigments (R-1, R-2, and R-3) at room temperature.

2, and R-3). The wall spectra reveal two doublets, D1 (Fe³⁺) and D2 (Fe²⁺), arising from quadrupole splitting in paramagnetic states. In the W-1 sample, the isomer shift (IS) values for D1 and D2 are 0.24 and 1.15 mm/s, respectively, with an area relative ratio (A) of 96:4, indicating a dominance of strongly covalent Fe³⁺ ions. D1, attributed to Fe3+ in soil, likely originates from amorphous ferrihydrite, superparamagnetic goethite (extremely small particle sizes or Al-substituted goethite), or iron within the silicate and clay mineral structures. Goethite, a common mineral in the environment, features octahedrally coordinated Fe(III) and can exist in a superparamagnetic state or as nanoparticles. Ferrihydrite, a poorly crystalline mineral, and superparamagnetic goethite exhibit non-magnetically ordered doublets at RT; however, VSM results only detected goethite in the walls. As the particle size of goethite decreases, aligning the electric field gradient (EFG) axis perpendicular to the spin direction, resulting in a superparamagnetic doublet with a quadrupole splitting (QS) value of 0.5-0.6 mm/s [26]. D2, attributed to Fe²⁺, likely arises from iron in Fe(II)bearing primary minerals. Thus, in Fig. 6a, the D1 (Fe³⁺) component primarily relates to superparamagnetic goethite and Fe(III)-bearing silicate minerals, whereas D2 (Fe²⁺) corresponds to structural iron in primary minerals, such as chlorite. In contrast, the RT Mössbauer spectra of red pigment samples exhibit an additional magnetic sextet alongside the D1 and D2 doublets (Fig. 6b). The hyperfine magnetic field ($H_{\rm hf}$) value of the sextet is 500 kOe and its QS and IS values are -0.10 and 0.32 mm/s, indicating it represents hematite [27]. Although hematite could not be clearly identified by XRD, Mössbauer spectroscopy provided conclusive evidence of its presence in the red pigment due to its high sensitivity to iron-bearing phases. Therefore, apart from the D1 and D2 components derived from the walls, the red color of the red pigment can be attributed to hematite. Table 2 lists the parameters obtained from the Mössbauer spectra. The identification of hematite as the main component of the red pigment carries significance not only scientifically but also culturally, as its presence in the Gaya tombs may be interpreted as reflecting symbolic and ritual practices

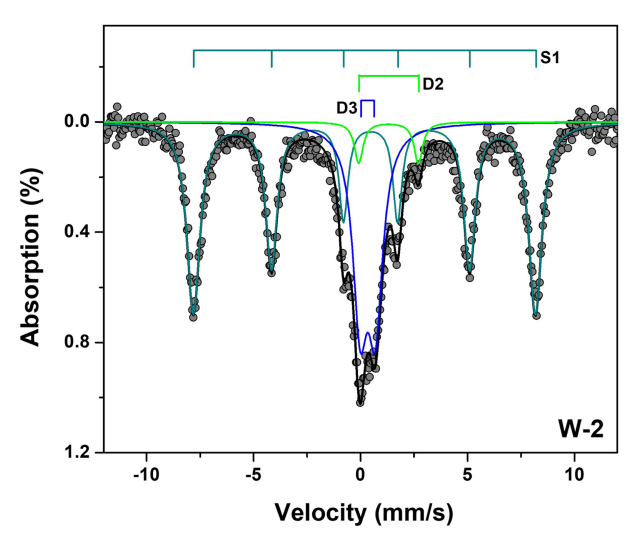


Fig. 7. (Color online) Mössbauer spectra of W-2 sample at 4.2 K.

embedded in their funerary traditions.

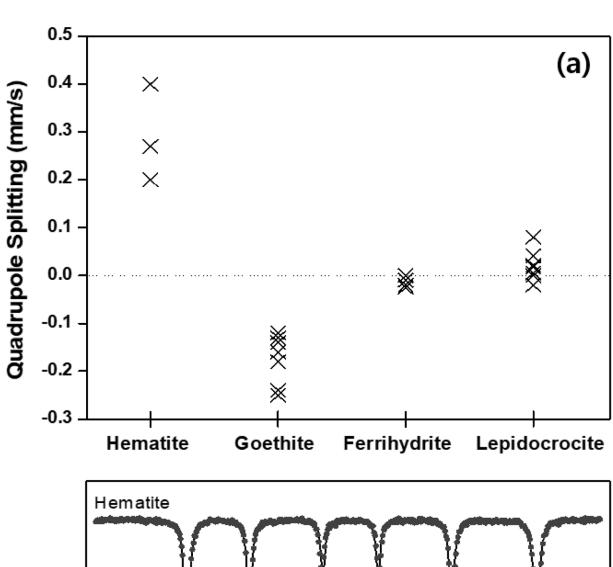
Furthermore, the Mössbauer spectrum of the W-2 sample at 4.2 K confirms the absence of ferrihydrite in the tomb walls and investigates the distribution of goethite content (Fig. 7). Unlike the RT Mössbauer spectrum, the spectrum measured at 4.2 K shows a reduction in the central resonance absorption area of D3 (Fe3+) and reveals an additional magnetic sextet (S1) due to hyperfine magnetic splitting. The S1 parameters are $H_{\rm hf}$ = 496.2 kOe, QS = -0.18 mm/s, and IS = 0.39 mm/s. The notably negative QS value at 4.2 K distinguishes S1 from ferrihydrite, which shows QS values near zero [28-30]. Therefore, S1 likely originates from superparamagnetic goethite. The $H_{\rm hf}$ value of S1 (496.2 kOe) is slightly lower than that of pure goethite at 4.2 K (506 kOe). This decrease is attributed to Fe³⁺ substitution by impurities, such as nonmagnetic Al³⁺ ions, in the goethite lattice, resulting in reduced particle size and crystallinity. At 4.2 K, D2 is attributed to Fe(II) in primary minerals, whereas D3 originates from structural Fe in Fe(III)-bearing silicate minerals. Consequently, D1 (96%) at RT comprises D3 (Fe(III)-bearing silicate minerals, 21%) and S1 (superparamagnetic goethite, 75%). The absence of ferrihydrite

Table 2. RT Mössbauer parameters of the red pigments (R-1, R-2, and R-3) and walls (W-1, W-2, and W-3).

Sample -	W-1		W-2		W-3		R-1		R-2			R-3			
	D1	D2	D1	D2	D1	D2	Hematite	D1	D2	Hematite	D1	D2	Hematite	D1	D2
IS (mm/s)	0.24	1.15	0.24	1.20	0.24	1.15	0.32	0.23	1.21	0.32	0.23	1.20	0.32	0.23	1.20
QS (mm/s)	0.62	2.13	0.62	2.18	0.62	2.13	-0.10	0.62	2.40	-0.10	0.62	2.30	-0.10	0.62	2.40
$H_{\rm hf}$ (kOe)	-	-	-	-	-	-	500.2	-	-	500.7	-	-	502.2	-	-
A (%)	96.06	3.94	95.82	4.18	96.43	3.57	40.87	55.83	3.30	42.17	52.40	5.43	43.60	53.05	3.35

and the exclusive presence of goethite in the tomb walls suggest that the interior of the tomb was not persistently humid over a long period and likely experienced some air exposure or maintained chemical stability.

Figure 8a shows the QS values for hematite, goethite, ferrihydrite, and lepidocrocite at 4.2–6 K, as summarized from previous studies [17, 28-33]. The QS value reflects the spin orientation and magnitude of the quadrupole interaction, which depends on the angle between the principal axis of the EFG and hyperfine magnetic field



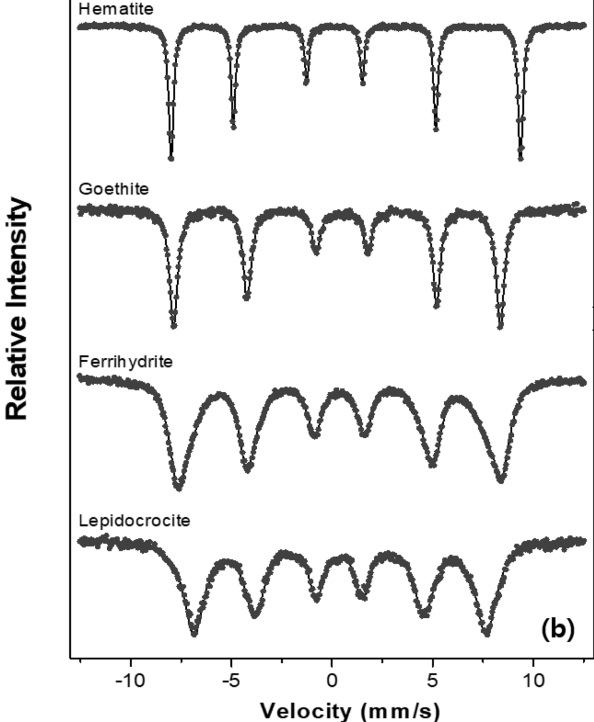


Fig. 8. (a) Quadrupole splitting values at 4.2–6 K, compiled from reported references [17, 28-33], and (b) ⁵⁷Fe Mössbauer spectra at 4.2 K for hematite, goethite, ferrihydrite, and lepidocrocite.

[34]. At RT, hematite displays a QS value from -0.2 to -0.1 mm/s, reflecting its canted antiferromagnetic state above the Morin transition temperature $(T_{\rm M})$. Above $T_{\rm M}$, the spin orientation aligns perpendicular to the c-axis ([111] axis) of its hexagonal structure. In contrast, below $T_{\rm M}$, hematite exhibits antiferromagnetic with a positive QS value (QS = 0.2-0.4 mm/s). At 4.2 K, bulk hematite has been reported to show a QS value of 0.4 mm/s, while nanosized hematite exhibits values in the range of 0.2-0.3 mm/s [22, 27]. These variations arise from differences in spin orientation. In bulk hematite, the spins are aligned parallel (0°) to the c-axis, whereas nanosized hematite maintains spins at a constant angle (28-29°) along the [110] axis. The EFG's anisotropic electric potential around the nucleus significantly influences the QS magnitude and sign. In Fig. 8a, goethite at 4.2 K exhibits a negative QS value, whereas that of ferrihydrite approaches zero. Goethite's high crystallinity positions Fe³⁺ ions in asymmetric octahedral coordination, resulting in a large EFG and a relatively low negative QS value [35]. Ferrihydrite has OS values close to zero because of a combination of factors, including mixed iron coordination environments (differences between tetrahedral and octahedral sites), disordered surface phase, and short-range-ordered Fe(III) [36]. Consequently, ferrihydrite likely does not exist in the W-2 sample, making the QS value a useful tool for distinguishing goethite from ferrihydrite. Lepidocrocite, formed through oxidative weathering of iron-bearing minerals, exhibits QS values from zero to low.

Figure 8b shows an example of the 57Fe Mössbauer spectrum at 4.2 K. Hematite exhibits highest $H_{\rm hf}$ value among all the iron oxides. Goethite has a lower $H_{\rm hf}$ value than hematite, which facilitates differentiation in soils where both minerals coexist. Ferrihydrite and lepidocrocite achieve complete magnetic ordering at 4.2 K, with lepidocrocite exhibiting the lowest $H_{\rm hf}$ value among magnetically ordered iron (oxy)hydroxides. Typically, mineral identification using Mössbauer spectroscopy involves measuring specific hyperfine parameters (IS, QS, and H_{hf}) and comparing them to reference values for accurate mineral identification. Ultimately, Mössbauer spectroscopy is a powerful tool for determining iron species, even in samples obscured by other mineral phases and indistinguishable from the background. However, it faces limitations related to temporal and spatial scales, including the complexity and heterogeneity of natural samples, as well as its reliance on phase identification from results obtained under cryogenic conditions. Despite these challenges, Mössbauer spectroscopy offers a critical advantage by enabling the detailed characterization of the magnetic and structural properties of various

iron oxides and (oxy)hydroxides. Notably, it has demonstrated the ability to identify iron oxides and minerals by comparing the QS values and $H_{\rm hf}$ values of each mineral. To build on this potential, future studies should investigate the magnetic behavior of iron oxides under diverse temperatures and environmental conditions, integrating complementary analytical techniques to comprehensively evaluate the properties of the samples from an archaeological perspective.

4. Conclusion

This study employed chromaticity measurements, XRD analysis, magnetic property, and Mössbauer spectroscopy to analyze the iron oxides and (oxy)hydroxides in the red pigment and walls of Tomb No. 63 of the ancient Gaya tumuli. XRD patterns identified the primary mineral in the samples and suggest the presence of amorphous or poorly crystalline phases in the walls. Magnetic property analysis further differentiated the iron oxides in the pigment and tomb walls. The red pigment exhibited weak ferromagnetic behavior characteristic of hematite, whereas the tomb walls displayed antiferromagnetic characteristics typical of goethite. Hysteresis curves from reference samples confirmed the magnetic behavior of the pigment and tomb walls aligned with that of hematite and goethite, respectively, without evidence of ferrihydrite. RT Mössbauer spectroscopy revealed a doublet attributed to Fe(III)bearing silicate minerals and superparamagnetic goethite and a doublet associated with Fe(II) in primary minerals in the tomb walls. In contrast, the Mössbauer spectrum of the red pigment displayed a sextet corresponding to hematite. Low-temperature (4.2 K) Mössbauer analysis of the tomb walls confirmed the presence of superparamagnetic goethite, ruling out ferrihydrite, suggesting that any initial ferrihydrite likely transformed over time. These results indicate that the tomb maintained a stable oxidative environment, enabling the crystallization of iron (oxy)hydroxides over extended periods. This study demonstrates the effectiveness of integrating multiple analytical techniques for mineral identification, particularly in archaeological contexts, emphasizing the role of QS values and hyperfine magnetic properties in distinguishing iron oxides and (oxy)hydroxides. Furthermore, Mössbauer spectroscopy has proven invaluable for detecting iron species even in complex matrices potentially obscured by other mineral phases, providing a deeper understanding of iron-based pigments in historical artifacts and soil transformations over time. Beyond mineralogical analysis, these findings highlight the cultural significance of red pigment in Gaya funerary practices, offering deeper insight into their traditions.

Acknowledgements

The authors would like to thank the Gaya National Research Institute of Cultural Heritage for providing the samples. This work was supported by the National Research Foundation of Korea (NRF) grant fund from the Korean government (MSIT) (No. NRF-2022R1A2C2092277) and the National Research Institute of Cultural Heritage grant funded by the Korea Heritage Service (No. RS-2021-NC100301).

References

- [1] W. R. Han, J. H. Kwon, J. Y. Park, and S. J. Kim, J. Conserv. Sci. **38**, 576 (2022).
- [2] J. Xiong, A. Li, C. Liu, J. Dong, B. Yang, J. Cao, and T. Ren, Energy Build. 251, 111388 (2021).
- [3] Y. N. Vodyanitskii, Eurasian Soil Sic. 43, 1244 (2010).
- [4] J. Torrent, R. Guzman, and M. A. Parra, Clay Clay Miner. **30**, 337 (1982).
- [5] Y. Cudennec and A. Lecerf, J. Solid State Chem. **179**, 716 (2006).
- [6] F. E. Furcas, B. Lothenbach, S. Mundra, C. N. Borca, C. C. Albert, O. B. Isgor, T. Huthwelker, and U. M. Angst, Environ. Sci. Technol. 57, 16097 (2023).
- [7] H. Liu, M. Ma, M. Qin, L. Yang, and Y. Wei, J. Solid State Chem. **183**, 2045 (2010).
- [8] K. Schulz, L. K. ThomasArrigo, R. Kaegi, and R. Kretzschmar, Environ. Sci. Technol. **56**, 5929 (2022).
- [9] K. Schulz, L. Notini, A. R. C. Grigg, and L. J. Kubeneck, Environ. Sci.: Processes Impacts **25**, 1945 (2023).
- [10] E. Dehouck, S. M. McLennan, E. C. Sklute, and M. D. Dyar, J. Geophys. Res. Planets. 122, 358 (2017).
- [11] M. Sassi, O. Qafoku, M. E. Bowden, C. I. Pearce, D. Latta, Q. R. S. Miller, M. D. Boamah, A. T. N'Diaye, J. E. Holliman Jr. E. Arenholz, and K. M. Rosso, Environ. Sci.: Nano 11, 1682 (2024).
- [12] M. Memon, K. S. Memon, M. S. Akhtar, and D. Stuben, Commun. Soil Sci. Plant Anal. 40, 162 (2009).
- [13] C. F. Holder, R. E. Schaak, ACS Nano 13, 7359 (2019).
- [14] L. Notini, K. Schulz, L. J. Kubeneck, A. R. C. Grigg, K. A. Rothwell, G. Fantappiè, L. K. ThomasArrigo, and R. Kretzschmar, Environ. Sci. Technol. 57, 10008 (2023).
- [15] E. Murad, Clay Miner. 45, 413 (2010).
- [16] R. E. Vandenberghe, E. de Grave, P. M. A. de Bakker, M. Krs, and J. J. Hus, Hyperfine Interact. **68**, 319 (1992).
- [17] J. T. Lim, C. S. Kim, D. H. Chun, and J. C. Park, J. Korean. Phys. Soc. **68**, 302 (2016).
- [18] Y. Sun, S. Yang, G. D. Sheng, and Q. Wang, Radiochim. Acta 100, 779 (2012).
- [19] X. Wang, M. Zhu, L. K. Koopal, W. Li, W. Xu, F. Liu, J. Zhang, Q. Liu, X. Feng, and D. L. Sparks, Environ. Sci.:

- Nano 3, 190 (2016).
- [20] Q. Liu, Y. Yu, J. Torrent, A. P. Roberts, Y. Pan, and R. Zhu, J. Geophys. Res. Solid Earth 111, B12S34 (2006).
- [21] E. Brok, C. Frandsen, D. E. Madsen, and H. Jacobsen, J. Phys. D Appl. Phys. 47, 365003 (2014).
- [22] M. Ounacer, A. Essoumhi, M. Sajieddine, A. Razouk, B. F. O. Costa, S. M. Dubiel, and M. Sahlaoui, J. Supercond. Nov. Magn. 33, 3249 (2020).
- [23] R. M. Hazen and R. Jeanloz, Rev. Geophys. 22, 37 (1984).
- [24] D. F. Valezi, C. E. A. Carneiro, A. C. S. Costa, A. Paesano Jr. J. C. Spadotto, I. G. Solórzano, O. M. Londoño, and E. Di Mauro, Mater. Chem. Phys. 246, 122851 (2020).
- [25] D. F. Valezi, J. T. Maeda, B. L. S. Vicentin, A. C. G. Mantovani, J. C. Spadotto, A. Urbano, F. F. Ivashita, A. Paesano Jr., C. J. Magon, and E. Di Mauro, Physica B Condens. Matter 650, 414537 (2023).
- [26] C. Frandsen, D. E. Madsen, C. B. Boothroyd, and S. Mørup, Croat. Chem. Acta 88, 481 (2015).
- [27] M. Mashlan, R. Zboril, L. Machala, M. Vujtek, J. Walla, and K. Nomura, J. Metestable Nanocryst. Mater. **20-21**, 641 (2004).
- [28] A. Bustamante, D. Lovera, R. Quille, A. V. Arias, and J.

- Quiñones, Hyper. Inter. 195, 63 (2010).
- [29] D. A. Balaev, S. V. Stolyar, Y. V. Knyazev, R. N. Yaroslavtsev, A. I. Pankrats, A. M. Vorotynov, A. A. Krasikov, D. A. Velikanov, O. A. Bayukov, V. P. Ladygina, and R. S. Iskhakov, Results Phys. 35, 105340 (2022).
- [30] F. B. Waanders, A. F. Mulaba-Bafubiandi, and F. Lodya, Hyper. Inter. 226, 721 (2014).
- [31] E. Murad and U. Schwertmann, Mineral. Mag. 48, 507 (1984).
- [32] T. S. Berquó, R. A. L. Imbernon, A. Blot, D. R. Franco, M. C. M. Toledo, and C. S. M. Partiti, Phys. Chem. Minerals 34, 287 (2007).
- [33] J. L. Bishop, C. M. Pieters, and R. G. Burns, Geoch. Cosm. Act. **57**, 4583 (1993).
- [34] A. Blachowski, K. Komedera, K. Ruebenbauer, G. Cios, J. Żukrowsski, and R. Górnicki, J. Alloys Comp. **673**, 420 (2016).
- [35] A. Meagher and Q. A. Pankhurst, Phys Stat Sol (a) **101**, K73 (1987).
- [36] J. M. Byrne and A. Kappler, Am. Mineral. **107**, 1643 (2022).